mathematics

MDPI

Article

Proposing an Intelligent Dual-Energy Radiation-Based System for Metering Scale Layer Thickness in Oil Pipelines Containing an Annular Regime of Three-Phase Flow

Osman Taylan [1], Mona Abusurrah [2], Saba Amiri [3], Ehsan Nazemi [4], Ehsan Eftekhari-Zadeh [5,*] and Gholam Hossein Roshani [6]

1 Department of Industrial Engineering, Faculty of Engineering, King Abdulaziz University, P.O. Box 80204, Jeddah 21589, Saudi Arabia; otaylan@kau.edu.sa
2 Department of Management Information Systems, College of Business Administration, Taibah University, P.O. Box 344, Al-Madinah 42353, Saudi Arabia; mabusurrah@taibahu.edu.sa
3 Razi University, Kermanshah 6714414971, Iran; s.amiri@razi.ac.ir
4 Imec-Vision Lab, Department of Physics, University of Antwerp, 2610 Antwerp, Belgium; ehsan.nazemi@uantwerpen.be
5 Institute of Optics and Quantum Electronics, Friedrich-Schiller-University Jena, Max-Wien-Platz 1, 07743 Jena, Germany
6 Electrical Engineering Department, Kermanshah University of Technology, Kermanshah 6715685420, Iran; hosseinroshani@kut.ac.ir
* Correspondence: e.eftekharizadeh@uni-jena.de

Citation: Taylan, O.; Abusurrah, M.; Amiri, S.; Nazemi, E.; Eftekhari-Zadeh, E.; Roshani, G.H. Proposing an Intelligent Dual-Energy Radiation-Based System for Metering Scale Layer Thickness in Oil Pipelines Containing an Annular Regime of Three-Phase Flow. *Mathematics* **2021**, *9*, 2391. https://doi.org/10.3390/math9192391

Academic Editor: Mario Versaci

Received: 8 September 2021
Accepted: 23 September 2021
Published: 26 September 2021

Abstract: Deposition of scale layers inside pipelines leads to many problems, e.g., reducing the internal diameter of pipelines, damage to drilling equipment because of corrosion, increasing energy consumption because of decreased efficiency of equipment, and shortened life, etc., in the petroleum industry. Gamma attenuation could be implemented as a non-invasive approach suitable for determining the mineral scale layer. In this paper, an intelligent system for metering the scale layer thickness independently of each phase's volume fraction in an annular three-phase flow is presented. The approach is based on the use of a combination of an RBF neural network and a dual-energy radiation detection system. Photo peaks of ^{241}Am and ^{133}Ba registered in the two transmitted detectors, and scale-layer thickness of the pipe were considered as the network's input and output, respectively. The architecture of the presented network was optimized using a trial-and-error method. The regression diagrams for the testing set were plotted, which demonstrate the precision of the system as well as correction. The MAE and RMSE of the presented system were 0.07 and 0.09, respectively. This novel metering system in three-phase flows could be a promising and practical tool in the oil, chemical, and petrochemical industries.

Keywords: scale-layer thickness; three-phase flow; volume fraction-independent; petroleum pipeline; dual-energy technique; radial basis function; neural network

1. Introduction

Deposition of scale layers inside pipelines leads to many problems in the petroleum industry. As a part of such problems, it can include decreasing of the internal diameter, drilling equipment corrosion, increasing the energy consumption due to decreased equipment efficiency, short life, and so forth. Water flooding, which contains calcium, barium, and strontium sulfate scales, has caused many scale problems in several oil fields worldwide. Scale deposition limits and blocks petroleum production. Consequently, scale deposition causes critical challenges such as emergency shutdowns, equipment failures, and decreasing efficiency of equipment [1–8].

Gamma attenuation technique is a useful method for detecting mineral scale in petroleum pipelines. In 2015 [7], Oliviera et al. employed a NaI detector together with a

^{137}Cs radioisotope source to scan scale deposits in a pipe. They acquired a gamma spectrum for each 0.5 cm step. They finally concluded that the gamma transmission scanning could estimate the presence of scale in a pipe in which a single-phase fluid flows, but that it is impossible to predict the precise distribution of scale. In 2018 [8], Teixeira et al. presented an approach to investigate scale in a pipe. The proposed geometry consisted of a steel pipe, a ^{137}Cs radioisotope source with isotropic flux, and one NaI detector. The gamma spectra measured from the pipe's internal diameter were considered the input of the ANN, whereas the output was the thickness of the scale. This methodology estimated the scale thickness with deviations below 10% for 70% of the cases. The drawback of their proposed system was that they could only measure the scale thickness of pipelines in which a single fluid flowed, while in real oil pipelines there exists two or three-phase flow. Roshani et al. investigated the possibility of identifying the flow regime and determining gas void fraction in two-phase flow without any dependency on the scale layer of the oil pipeline by combining photon attenuation and artificial intelligence techniques [9]. Their study implemented ANN for regime identification and void fraction prediction. The results revealed that their proposed technique is unable to identify all three flow regimes. To the best of the author's knowledge, as mentioned in the literature review, no investigation has been done on the thickness measurement of scale layers in oil pipelines with an existing gas–oil–water three-phase flow with various volume fractions. In real situations, there are two or three-phase flows with variating volume fractions inside the oil pipelines which affect drastically the performance of radiation-based scale thickness meters. The novelty of the present study is the proposal of a system with the capability to measure scale layer thickness in petroleum and oil pipelines without any dependency on the volume fractions of each phase in the annular regime of a three-phase flow. We employed a dual-energy gamma attenuation technique combined with a radial basis function neural network (RBFNN) to achieve this aim. The details of the proposed approach are explained in the following sections.

2. Materials and Methods

2.1. Monte Carlo Simulation

MCNP code [10] was implemented in the present investigation to model the radiation-based system. In the past few decades, it has been proved that MCNP code is a potential tool for modeling radiation-based measuring instruments [11–22]. As pointed out in the abstract section, our aim is to propose a gamma radiation-based system with the ability to determine scale thickness independently of volume fraction changes of an annular three-phase flow's components. In order to obtain more information from the different materials inside the pipe, a system consisting of a dual-energy source consisting of ^{241}Am and ^{133}Ba radioisotopes that emit photons with energies of 59 and 356 keV, respectively, and two NaI detectors for recording transmitted photons were used.

As shown in Figure 1, a steel pipe with an internal radius of 10 cm was simulated in this study. In order to model the scale layer, a cylindrical shell of barium sulfate (BaSO4) with a density of 4.5 g.cm^{-3} and different thicknesses in the range of 0–2 cm was considered on the internal wall of the steel pipe.

An annular regime of a three-phase flow, including gas, oil, and water components, was modeled inside the pipe. Air, gasoil, and water were utilized as gas, oil, and water phases, respectively. Various volume fractions (10–80 percent) were simulated for each component (5 different scale thickness $\times$ 36 different volume fractions = total of 180 simulations performed) for each scale thickness.

As mentioned earlier, in this investigation, two NaI detectors were applied. Tally F8 was utilized to register photon energy spectra in both detectors. The first detector was positioned diametrically in front of the radioactive source, and the second one was placed at an orientation of 7°.

It is worth mentioning that the simulated configuration performance in this work was benchmarked in our earlier study using an experiment [23]. As shown in Figure 2, in that study, an experimental model was established. A two-phase flow annular regime with various amounts of gas and oil components was also modeled inside a pipe. A geometry the same as the experimental setup was simulated. The acquired results showed that the experimental and simulated data were in good agreement, which confirmed the simulated detection system performance.

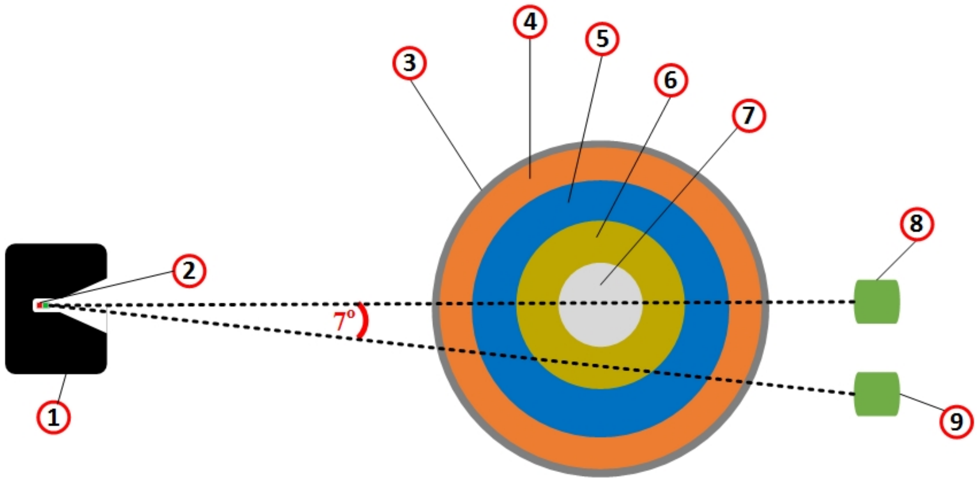

Figure 1. Simulated geometry: (1) Radiation shield, (2) Radioactive sources, (3) Steel pipe, (4) Scale layer, (5) Water phase, (6) Oil phase, (7) Gas phase, (8) First transmission detector, (9) Second transmission detector.

Although the presented system in the current study was developed for measuring the scale layer thickness independently of different volume fractions of each phase in an annular regime of a three-phase flow, it can be applied for the other types of flow regimes.

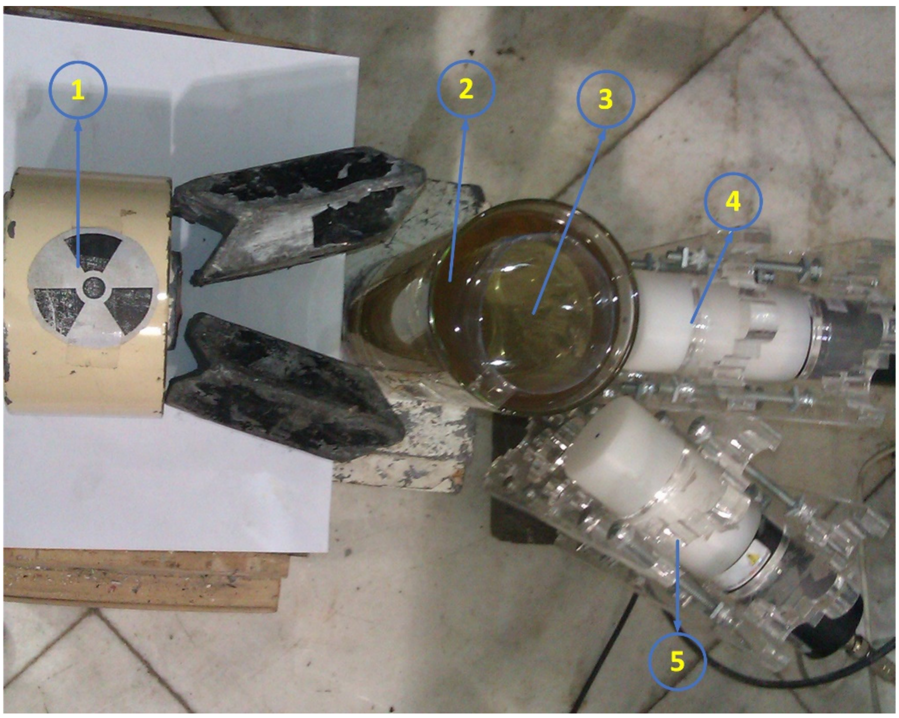

Figure 2. Experimental setup: (1) Radioisotope source, (2) Oil phase, (3) Gas phase, (4) 1st detector, (5) 2nd detector [20].

2.2. Radial Basis Function (RBF) Neural Networks

In recent years, a variety of advanced computational methods, e.g., finite element, Newton's method, numerical linear algebra, statistics, numerical analysis, discrete Fourier transform, tensor analysis, and artificial intelligence, have been used in different research fields such as material engineering [24–31], chemical engineering [32–37], electrical engineering [38–46], medical and biomedical sciences [47–52], civil engineering [53–56], economic science [57–68], fluid mechanic engineering [69–76], computer and information technology engineering [77–79], physics [80,81], petroleum engineering [82–90], etc. Among them, it has been proven that ANN is the most powerful tool for classification and prediction. ANNs consist of three distinct layers: input, hidden, and output layers. Different kinds of ANNs consist of one or several hidden layers, but RBF neural networks have only one hidden layer. An RBF neural network was used in the present study, while in most of the previous relevant studies, other types of ANNs such as MLP [8,11,14] and GMDH [13,15,55] were used. The advantage of RBF is that its training process, with only three layers, is normally faster than other types of ANN models because of its simpler structure. MLP networks initially use randomly generated parameters, but for RBF neural networks, it is necessary to set correct initial states.

There are different numbers of computational units named neurons in each layer. RBF networks weigh and combine information through these neurons. Concerning process input data, RBF is used in the hidden layer of the RBF neural network. A typical architecture of an RBF neural network is shown in Figure 3. The hidden neurons, through "synaptic weights", connect and weigh the input signals. The neurons' responses represent neuron "activation" values. Nonlinear activation functions consider such values by adding up a bias to the weighted summation of their input [91].

$$y = \sum(\text{weight} * \text{input}) + \text{bias} \tag{1}$$

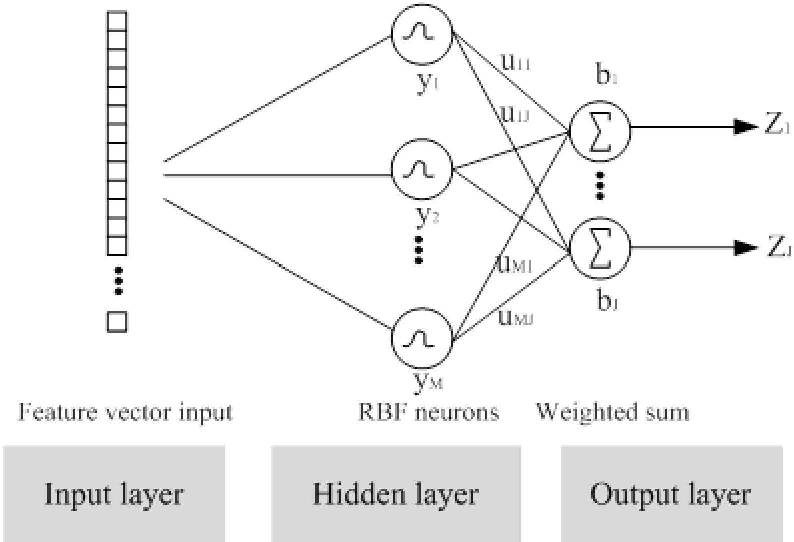

Figure 3. Typical architecture of an RBF neural network.

The activation function of the hidden layer is "radbas". Therefore, Equation (2) refers to the hidden layer, and precisely to the mth node's output [91–93]:

$$y_m = e^{\left(-\frac{||x-v_m||^2}{2\sigma_m{}^2}\right)} \tag{2}$$

The default spread value (σ) in MATLAB software commands is 1, but this value was optimized in this study. The output prediction from the jth node of the output layer is [94]:

$$z_j = \sum_{m=1}^{M} u_{mj} y_m + b_j \quad (3)$$

Both "radbas" and "purelin" are neural transfer functions. These kinds of functions are the most well-known functions for the hidden layer and output layer of typical RBF neural networks, respectively, and have been used in a lot of previous research. In this study, 180 separate cases were simulated using the MCNPX code. 126 cases (70%) were implemented to train the network, and 54 cases (30%) were used to test the efficiency of the presented RBF neural network. In this problem, for measuring the scale layer thickness of pipe independently of different volume fractions in a three-phase flow, four features were extracted from two transmission detectors and applied to the RBF neural network. The counts under the photopeaks for ^{241}Am and ^{133}Ba from both transmission detectors were considered the RBF neural network inputs, and scale layer thickness of the pipe was considered the RBF neural network output. The reason for choosing these mentioned features as the inputs for the network is that counts under these two photopeaks are directly connected to the amount and type of materials between the radiation source and the detector, while other features in the recorded photon energy spectrum inside the detector are not directly connected. The procedure for scale layer thickness metering is illustrated in Figure 4.

Using a trial-and-error method, the best configuration of the network was obtained. As mentioned previously, the RBF neural network has only 3 layers. The obtained configuration was tabulated in Table 1, and the schematic of the network is shown in Figure 5.

Table 1. Configuration of the proposed ANN.

ANN Type	RBF Neural Network
Function used for network performance evaluation	'mse'
Activation function	'radbas'
Spread of radial basis functions	2
Number of layers	3
Number of neurons	11
Mean squared error goal	0

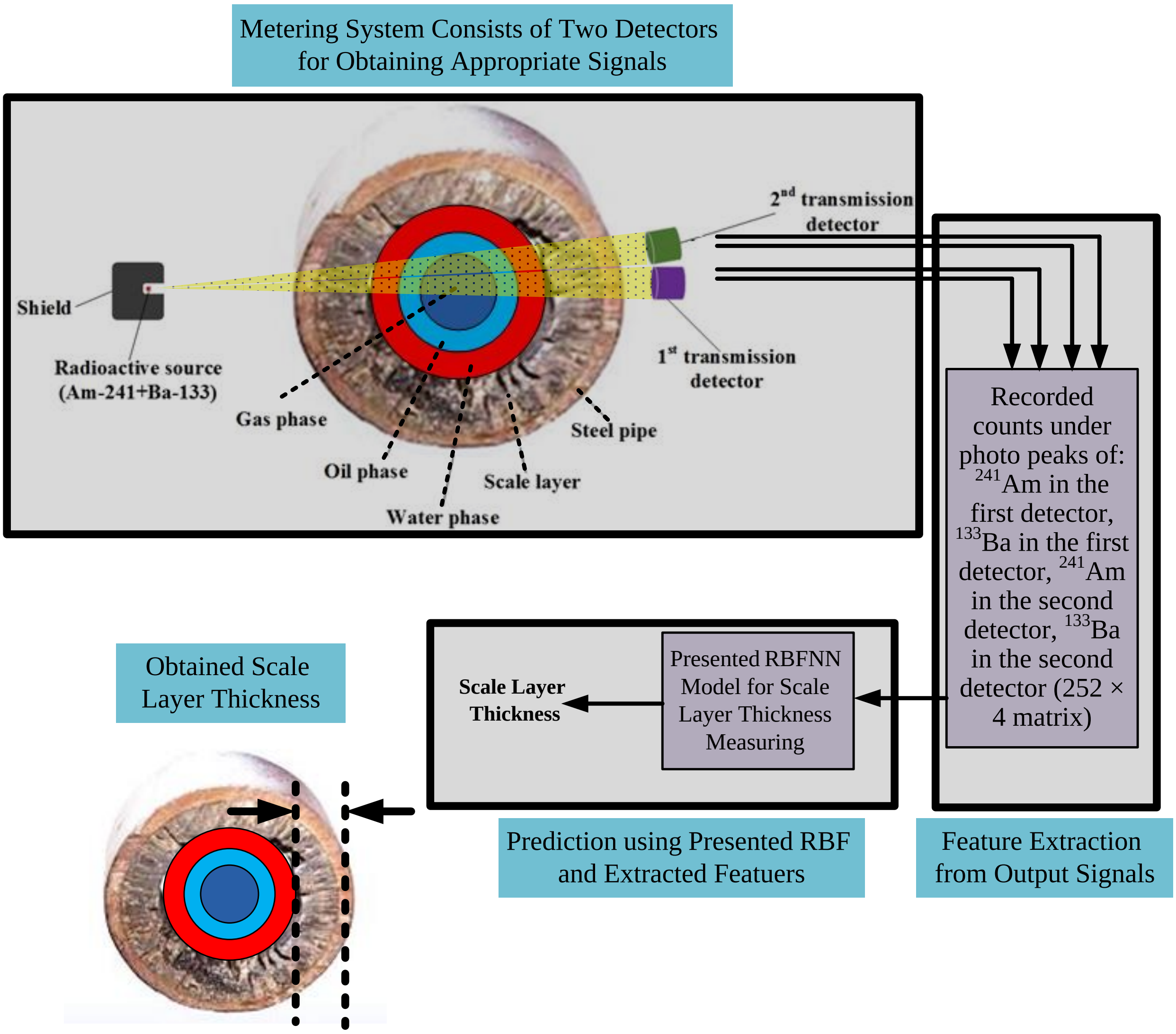

Figure 4. The conceptual procedure for scale layer thickness metering.

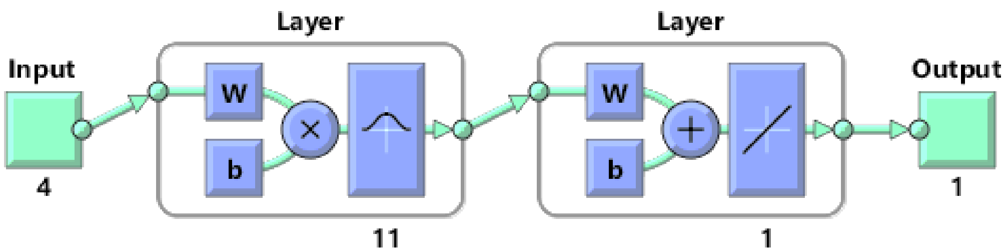

Figure 5. Schematic for the optimized RBF neural network.

3. Results

3.1. Performance of the Modeled Detection System

Counts under photo peaks of ^{241}Am and ^{133}Ba radioisotopes were recorded in both detectors for various scale layer thicknesses and volume fractions. As an example, ternary surface plots of the recorded counts under the photopeak for the ^{133}Ba radioisotope in the first detector for various combinations of gas, oil, and water volume fractions when the scale thickness is 0 and 2 cm, are shown in Figure 6a,b. Comparing Figure 6a,b, it could be observed that when the scale layer is 0 cm, the sensitivity relative to changes of gas, oil, and water components is much more than when the scale thickness is 2 cm. In other words, by increasing the thickness of the scale layer, somehow, information about the flow inside the pipe starts fading. This exact occurrence has also been observed for the other detector and radioisotope.

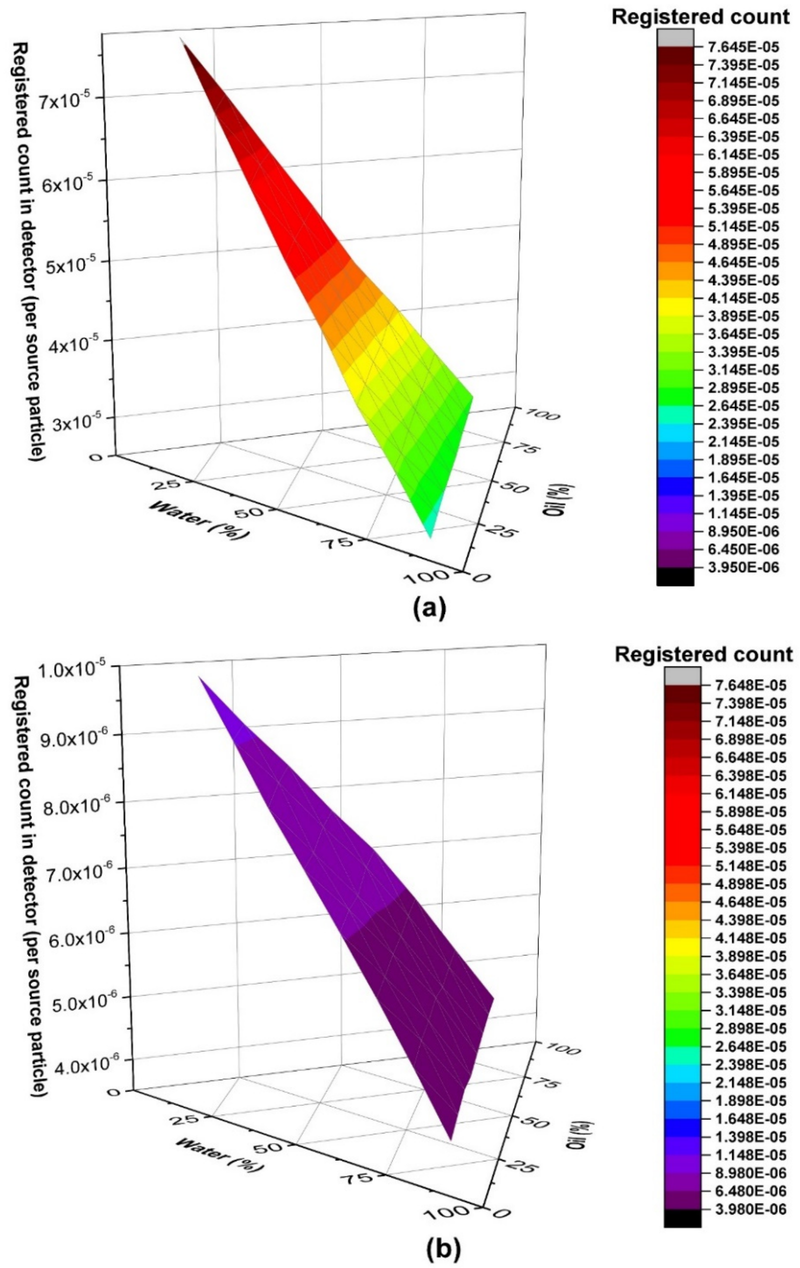

Figure 6. Recorded counts under the photopeak for the ^{133}Ba radioisotope in the 1st detector for various combinations of volume fractions when the scale thickness is: (**a**) 0 cm, (**b**) 2 cm.

For example, registered counts in both detectors versus the changes in scale thickness for the state in which the volume fractions of components are fixed (50% gas, 30% oil, and 20% water) are shown in Figure 7. As expected, the registered counts in both detectors decrease by increasing the scale thickness. As can be seen from Figure 7, the sensitivity of registered counts under the photopeak for the ^{133}Ba radioisotope in both detectors relative to the scale thickness changes is more than those for ^{241}Am.

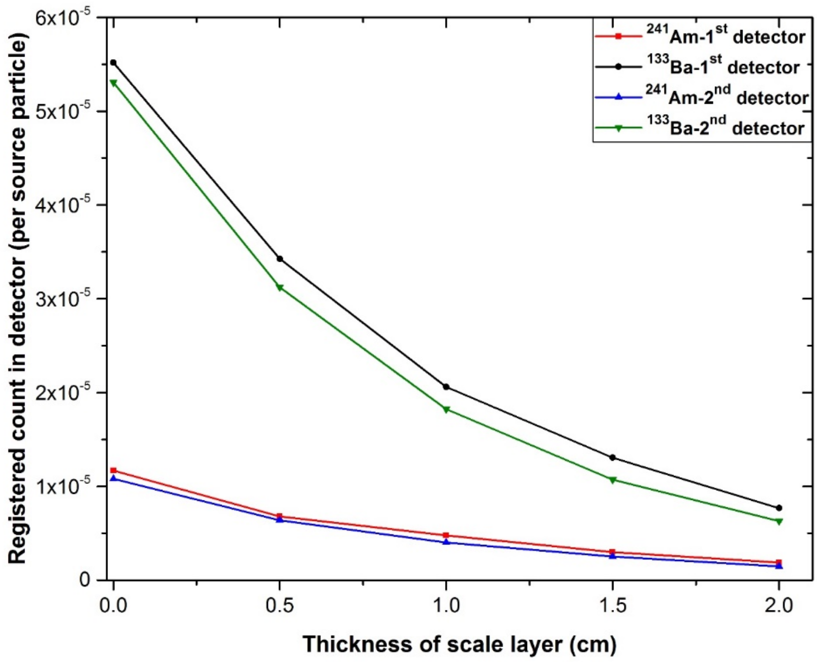

Figure 7. Registered counts in both detectors versus the changes in scale thickness for the state in which the volume fractions of components are fixed (50% gas, 30% oil, and 20% water).

3.2. Scale Thickness Prediction by RBF Neural Networks

The input matrix, output matrix (network target), and measured data (network output) for the testing set (54 cases) were tabulated in Table 2. An Intel Core i7 CPU computer was used for running the MCNPX simulations and MATLAB 8.1.0.604 software. The acquired results are shown as regression diagrams for training and testing sets in Figure 8a,b. In this figure, measured scale values versus real scale values have been plotted for both training and testing sets.

Table 2. The input matrix, output matrix, and measured data (network output) for the testing set (54 cases).

Data Number	^{241}Am Peak in First Detector	^{133}Ba Peak in First Detector	^{241}Am Peak in Second Detector	^{133}Ba Peak in Second Detector	Scale Layer Thickness (cm)	Measured Scale Layer Thickness	Difference between Real and Measured Thickness
1	7.50×10^{-6}	2.63×10^{-5}	6.37×10^{-6}	1.84×10^{-5}	0	−0.199	0.198999
2	7.19×10^{-6}	2.81×10^{-5}	6.26×10^{-6}	2.01×10^{-5}	0	0.053158	0.053158
3	8.37×10^{-6}	3.28×10^{-5}	7.46×10^{-6}	2.89×10^{-5}	0	0.060322	0.060322
4	9.03×10^{-6}	3.55×10^{-5}	7.48×10^{-6}	3.13×10^{-5}	0	0.017096	0.017096
5	9.54×10^{-6}	4.04×10^{-5}	8.77×10^{-6}	3.79×10^{-5}	0	0.111143	0.111143
6	1.06×10^{-5}	4.68×10^{-5}	1.02×10^{-5}	4.40×10^{-5}	0	−0.00335	0.003347
7	1.03×10^{-5}	4.83×10^{-5}	9.83×10^{-6}	4.64×10^{-5}	0	0.159976	0.159976
8	1.14×10^{-5}	5.60×10^{-5}	1.10×10^{-5}	5.40×10^{-5}	0	0.028774	0.028774
9	1.23×10^{-5}	6.31×10^{-5}	1.21×10^{-5}	6.04×10^{-5}	0	−0.02497	0.024969
10	3.84×10^{-6}	1.56×10^{-5}	3.27×10^{-6}	1.09×10^{-5}	0.5	0.597286	0.097286
11	4.45×10^{-6}	1.81×10^{-5}	3.50×10^{-6}	1.25×10^{-5}	0.5	0.557677	0.057677
12	5.19×10^{-6}	1.97×10^{-5}	4.23×10^{-6}	1.61×10^{-5}	0.5	0.546581	0.046581
13	5.19×10^{-6}	2.21×10^{-5}	4.20×10^{-6}	1.86×10^{-5}	0.5	0.784895	0.284895
14	5.54×10^{-6}	2.53×10^{-5}	5.08×10^{-6}	2.16×10^{-5}	0.5	0.65492	0.15492
15	6.35×10^{-6}	2.64×10^{-5}	5.36×10^{-6}	2.33×10^{-5}	0.5	0.495023	0.004977
16	6.33×10^{-6}	2.96×10^{-5}	5.68×10^{-6}	2.68×10^{-5}	0.5	0.569258	0.069258
17	6.97×10^{-6}	3.37×10^{-5}	6.42×10^{-6}	3.08×10^{-5}	0.5	0.484072	0.015928
18	7.81×10^{-6}	3.74×10^{-5}	7.19×10^{-6}	3.52×10^{-5}	0.5	0.446271	0.053729

Table 2. *Cont.*

Data Number	^{241}Am Peak in First Detector	^{133}Ba Peak in First Detector	^{241}Am Peak in Second Detector	^{133}Ba Peak in Second Detector	Scale Layer Thickness (cm)	Measured Scale Layer Thickness	Difference between Real and Measured Thickness
19	9.43×10^{-6}	4.63×10^{-5}	8.84×10^{-6}	4.49×10^{-5}	0.5	0.362445	0.137555
20	2.61×10^{-6}	1.01×10^{-5}	2.08×10^{-6}	6.59×10^{-6}	1	1.03317	0.03317
21	2.82×10^{-6}	1.09×10^{-5}	2.01×10^{-6}	6.87×10^{-6}	1	1.022872	0.022872
22	2.85×10^{-6}	1.16×10^{-5}	2.07×10^{-6}	7.32×10^{-6}	1	1.029416	0.029416
23	3.18×10^{-6}	1.27×10^{-5}	2.76×10^{-6}	9.63×10^{-6}	1	0.983388	0.016612
24	3.22×10^{-6}	1.35×10^{-5}	2.75	1.06×10^{-5}	1	0.706746	0.293254
25	3.72×10^{-6}	1.51×10^{-5}	3.34×10^{-6}	1.24×10^{-5}	1	0.93631	0.06369
26	3.58×10^{-6}	1.55×10^{-5}	3.22×10^{-6}	1.30×10^{-5}	1	1.141341	0.141341
27	4.40×10^{-6}	1.75×10^{-5}	4.14×10^{-6}	1.77×10^{-5}	1	1.068921	0.068921
28	4.01×10^{-6}	1.81×10^{-5}	3.75×10^{-6}	1.56×10^{-5}	1	1.052691	0.052691
29	4.79×10^{-6}	1.97×10^{-5}	4.05×10^{-6}	1.78×10^{-5}	1	0.914527	0.085473
30	4.72×10^{-6}	2.08×10^{-5}	4.19×10^{-6}	1.85×10^{-5}	1	0.926637	0.073363
31	5.61×10^{-6}	2.53×10^{-5}	5.05×10^{-6}	2.36×10^{-5}	1	0.732584	0.267416
32	1.63×10^{-6}	6.64×10^{-6}	1.25×10^{-6}	3.95×10^{-6}	1.5	1.575543	0.075543
33	1.82×10^{-6}	6.81×10^{-6}	1.33×10^{-6}	4.12×10^{-6}	1.5	1.496197	0.003803
34	1.92×10^{-6}	7.31×10^{-6}	1.41×10^{-6}	4.45×10^{-6}	1.5	1.439766	0.060234
35	2.11×10^{-6}	8.29×10^{-6}	1.63×10^{-6}	6.01×10^{-6}	1.5	1.590924	0.090924
36	2.12×10^{-6}	8.71×10^{-6}	1.74×10^{-6}	6.39×10^{-6}	1.5	1.560707	0.060707
37	2.36×10^{-6}	9.81×10^{-6}	2.01×10^{-6}	7.67×10^{-6}	1.5	1.532757	0.032757
38	2.44×10^{-6}	1.03×10^{-5}	2.07×10^{-6}	8.21×10^{-6}	1.5	1.562431	0.062431
39	2.70×10^{-6}	1.14×10^{-5}	2.31×10^{-6}	9.21×10^{-6}	1.5	1.460378	0.039622
40	3.01×10^{-6}	1.27×10^{-5}	2.48×10^{-6}	1.06×10^{-5}	1.5	1.469839	0.030161
41	3.18×10^{-6}	1.40×10^{-5}	2.67×10^{-6}	1.19×10^{-5}	1.5	1.47086	0.02914
42	3.60×10^{-6}	1.58×10^{-5}	3.04×10^{-6}	1.37×10^{-5}	1.5	1.339425	0.160575
43	9.37×10^{-7}	4.12×10^{-6}	7.45×10^{-7}	2.52×10^{-6}	2	2.07488	0.07488
44	1.07×10^{-6}	4.21×10^{-6}	8.20×10^{-7}	2.60×10^{-6}	2	1.997739	0.002261
45	1.15×10^{-6}	4.49×10^{-6}	8.91×10^{-7}	2.77×10^{-6}	2	1.932604	0.067396
46	1.21×10^{-6}	5.07×10^{-6}	9.96×10^{-7}	3.36×10^{-6}	2	1.944003	0.055997
47	1.34×10^{-6}	5.22×10^{-6}	1.02×10^{-6}	3.64×10^{-6}	2	1.9735	0.0265
48	1.37×10^{-6}	5.76×10^{-6}	1.17×10^{-6}	4.35×10^{-6}	2	1.999857	0.000143
49	1.48×10^{-6}	6.08×10^{-6}	1.24×10^{-6}	4.65×10^{-6}	2	1.966943	0.033057
50	1.55×10^{-6}	6.58×10^{-6}	1.31×10^{-6}	5.28×10^{-6}	2	2.028499	0.028499
51	1.68×10^{-6}	7.01×10^{-6}	1.36×10^{-6}	5.51×10^{-6}	2	1.961872	0.038128
52	1.86×10^{-6}	7.45×10^{-6}	1.43×10^{-6}	6.28×10^{-6}	2	2.048818	0.048818
53	2.04×10^{-6}	8.38×10^{-6}	1.53×10^{-6}	7.11×10^{-6}	2	2.040112	0.040112
54	2.40×10^{-6}	9.89×10^{-6}	1.87×10^{-6}	8.89×10^{-6}	2	1.984083	0.015917

For one output of the proposed RBF neural network model, the defined errors are shown in Table 3. Those defined errors contain MAE and RMSE, which have been calculated as:

$$\mathrm{MAE} = \frac{1}{N}\sum_{i=1}^{N}|X_i(real) - X_i(measured)| \tag{4}$$

$$\mathrm{RMSE} = \sqrt{\frac{\sum_{j=1}^{N}(X_j(real) - X_j(measured))^2}{N}} \tag{5}$$

where the number of data points is referred to by N, '*X (real)*' and '*X (measured)*' applies for actual values and RBF predicted values, respectively.

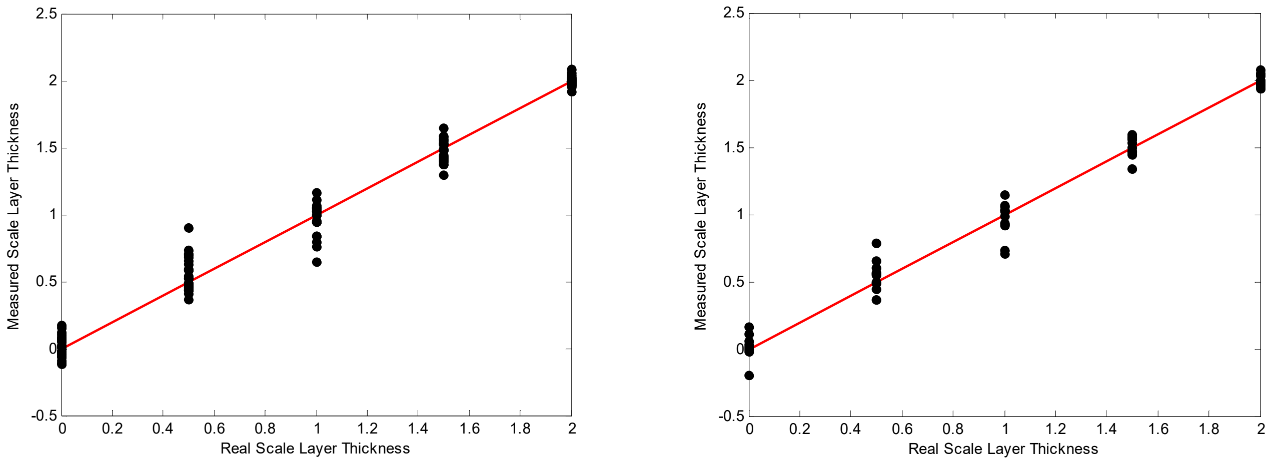

(**a**) (**b**)

Figure 8. Measured scale value versus real data for (**a**) training and (**b**) testing sets.

Table 3. Errors of the designed RBF neural network.

Error	Training Data	Testing Data
MAE	0.067	0.070
RMSE	0.095	0.097

Network performance testing using training and test data sets will give the reassurance of avoiding under-fitting and over-fitting of problems. For evaluating the precision and accuracy of the proposed network, the MAE and RMSE were calculated in Table 3. By investigating the errors ratio, it is clear that the errors are lower—proving the validity of the ANN model, which is well-trained and doesn't encounter under-fitting or over-fitting of the problem. The low errors for the training set show that the under-fitting problem has not occurred and that the network is precise. A performance-comparative evaluation of the RBF neural network with other ANN types for use in the presented metering system is proposed for future works.

4. Conclusions

In the present investigation, an intelligent system for metering the scale layer thickness independently of each phase's volume fractions in an annular three-phase flow was presented. In this regard, a combination of an RBF neural network and a Monte Carlo-based radiation transport calculation method was used. Photo peaks of ^{241}Am and ^{133}Ba from two transmitted detectors and the scale layer thickness of the pipe were considered the inputs and output of the network. The architecture of the presented network was optimized using a trial-and-error method. The regression diagrams showed the precision of the system as well as correction. The MAE and RMSE of the presented system were 0.07 and 0.09, respectively. The reasonable obtained results demonstrate the robustness of the proposed system. As mentioned earlier, to the best knowledge of the authors, it is the first time that a radiation-based system with the ability to measure the thickness of scale layer in oil pipelines with an existing gas–oil–water three-phase flow with different volume fractions is presented. The proposed new metering system can be applied as a promising tool in the different industries for measuring the scale layer thickness of pipelines.

Author Contributions: Conceptualization, G.H.R. and O.T.; Software, G.H.R., S.A. and O.T.; Writing—Review and Editing, M.A., S.A., E.N., E.E.-Z. and O.T.; Funding acquisition, M.A., O.T. and E.E.-Z. All authors have read and agreed to the published version of the manuscript.

Funding: We acknowledge support from the German Research Foundation and the Open Access Publication Fund of the Thueringer Universitaets und Landesbibliothek Jena Projekt-Nr. 433052568. The Deanship of Scientific Research (DSR) at King Abdulaziz University, Jeddah, Saudi Arabia has funded this project, under grant no. (FP-13-43).

Institutional Review Board Statement: Not applicable.

Informed Consent Statement: Not applicable.

Data Availability Statement: Data is contained within the article.

Conflicts of Interest: The authors declare no conflict of interest.

References

1. Bahadori, A.; Zahedi, G.; Zendehboudi, S. Estimation of potential barium sulfate (barite) precipitation in oilfield brines using a simple predictive tool. *Environ. Prog. Sustain. Energy* **2013**, *32*, 860–865. [CrossRef]
2. BinMerdhah, A.B. Inhibition of barium sulfate scale at high-barium formation water. *J. Pet. Sci. Eng.* **2012**, *90–91*, 124–130. [CrossRef]
3. Zabihi, R.; Schaffie, M.; Nezamabadi-Pour, H.; Ranjbar, M. Artificial neural network for permeability damage prediction due to sulfate scaling. *J. Pet. Sci. Eng.* **2011**, *78*, 575–581. [CrossRef]
4. Candeias, J.; De Oliveira, D.; Dos Anjos, M.; Lopes, R. Scale analysis using X-ray microfluorescence and computed radiography. *Radiat. Phys. Chem.* **2013**, *95*, 408–411. [CrossRef]
5. Oliveira, D.F.; Santos, R.S.; Machado, A.S.; Silva, A.S.; Anjos, M.J.; Lopes, R.T. Characterization of scale deposition in oil pipelines through X-Ray Microfluorescence and X-Ray microtomography. *Appl. Radiat. Isot.* **2019**, *151*, 247–255. [CrossRef] [PubMed]
6. Abdul-Majid, S. Determination of wax deposition and corrosion in pipelines by neutron back diffusion collimation and neutron capture gamma rays. *Appl. Radiat. Isot.* **2013**, *74*, 102–108. [CrossRef]
7. Oliveira, D.F.; Nascimento, J.R.; Marinho, C.A.; Lopes, R.T. Gamma transmission system for detection of scale in oil exploration pipelines. *Nucl. Instrum. Methods Phys. Res. Sect. A Accel. Spectrometers, Detect. and Assoc. Equip.* **2015**, *784*, 616–620. [CrossRef]
8. Teixeira, T.P.; Salgado, C.M.; Dam, R.S.D.F.; Salgado, W.L. Inorganic scale thickness prediction in oil pipelines by gamma-ray attenuation and artificial neural network. *Appl. Radiat. Isot.* **2018**, *141*, 44–50. [CrossRef]
9. Roshani, M.; Phan, G.T.; Ali, P.J.M.; Roshani, G.H.; Hanus, R.; Duong, T.; Corniani, E.; Nazemi, E.; Kalmoun, E.M. Eval-uation of flow pattern recognition and void fraction measurement in two phase flow independent of oil pipeline's scale layer thickness. *Alex. Eng. J.* **2021**, *60*, 1955–1966. [CrossRef]
10. Pelowitz, D.B. *MCNP-X TM User's Manual, Version 2.5.0.*; LA-CP-05e0369; Los Alamos National Laboratory: Los Alamos, CA, USA, 2005.
11. Nazemi, E.; Feghhi, S.A.H.; Roshani, G.H.; Peyvandi, R.G.; Setayeshi, S. Precise Void Fraction Measurement in Two-phase Flows Independent of the Flow Regime Using Gamma-ray Attenuation. *Nucl. Eng. Technol.* **2016**, *48*, 64–71. [CrossRef]
12. Dai, T.; Cao, L.; He, Q.; Wu, H.; Shen, W. A Two-Way Neutronics/Thermal-Hydraulics Coupling Analysis Method for Fusion Blankets and Its Application to CFETR. *Energies* **2020**, *13*, 4070. [CrossRef]
13. Roshani, M.; Phan, G.; Roshani, G.H.; Hanus, R.; Nazemi, B.; Corniani, E.; Nazemi, E. Combination of X-ray tube and GMDH neural network as a nondestructive and potential technique for measuring characteristics of gas-oil–water three phase flows. *Measurement* **2021**, *168*, 108427. [CrossRef]
14. Salgado, C.M.; Pereira, C.M.N.A.; Schirru, R.; Brandao, L.E.B. Flow regime identification and volume fraction prediction in mul-tiphase flows by means of gamma-ray attenuation and artificial neural networks. *Prog. Nucl. Energy* **2010**, *52*, 555–562. [CrossRef]
15. Roshani, M.; Sattari, M.A.; Ali, P.J.M.; Roshani, G.H.; Nazemi, B.; Corniani, E.; Nazemi, E. Application of GMDH neural network technique to improve measuring precision of a simplified photon attenuation based two-phase flowmeter. *Flow Meas. Instrum.* **2020**, *75*, 101804. [CrossRef]
16. Salgado, C.; Brandão, L.; Conti, C.; Salgado, W. Density prediction for petroleum and derivatives by gamma-ray attenuation and artificial neural networks. *Appl. Radiat. Isot.* **2016**, *116*, 143–149. [CrossRef] [PubMed]
17. Roshani, M.; Phan, G.; Faraj, R.H.; Phan, N.-H.; Roshani, G.H.; Nazemi, B.; Corniani, E.; Nazemi, E. Proposing a gamma radiation based intelligent system for simultaneous analyzing and detecting type and amount of petroleum by-products. *Nucl. Eng. Technol.* **2021**, *53*, 1277–1283. [CrossRef]
18. El Abd, A. Intercomparison of gamma ray scattering and transmission techniques for gas volume fraction measurements in two phase pipe flow. *Nucl. Instrum. Methods Phys. Res. Sect. A Accel. Spectrom. Detect. Assoc. Equip.* **2014**, *735*, 260–266. [CrossRef]
19. Faghihi, R.; Nematollahi, M.; Erfaninia, A.; Adineh, M. Void fraction measurement in modeled two-phase flow inside a vertical pipe by using polyethylene phantoms. *Int. J. Hydrogen Energy* **2015**, *40*, 15206–15212. [CrossRef]
20. Roshani, G.H.; Feghhi, S.A.H.; Adineh-Vand, A.; Khorsandi, M. Application of adaptive neuro-fuzzy inference system in prediction of fluid density for a gamma ray densitometer in petroleum products monitoring. *Measurement* **2013**, *46*, 3276–3281. [CrossRef]

21. Yadollahi, A.; Nazemi, E.; Zolfaghari, A.; Ajorloo, A. Application of artificial neural network for predicting the optimal mixture of radiation shielding concrete. *Prog. Nucl. Energy* **2016**, *89*, 69–77. [CrossRef]
22. Yadollahi, A.; Nazemi, E.; Zolfaghari, A.; Ajorloo, A. Optimization of thermal neutron shield concrete mixture using artificial neural network. *Nucl. Eng. Des.* **2016**, *305*, 146–155. [CrossRef]
23. Nazemi, E.; Roshani, G.H.; Feghhi, S.A.H.; Setayeshi, S.; Zadeh, E.E.; Fatehi, A. Optimization of a method for identifying the flow regime and measuring void fraction in a broad beam gamma-ray attenuation technique. *Int. J. Hydrog. Energy* **2016**, *41*, 7438–7444. [CrossRef]
24. Versaci, M.; Morabito, F.C. Image Edge Detection: A New Approach Based on Fuzzy Entropy and Fuzzy Divergence. *Int. J. Fuzzy Syst.* **2021**, *23*, 918–936. [CrossRef]
25. Mokhtari, S.; Skelly, K.D.; Krull, E.A.; Coughlan, A.; Mellott, N.P.; Gong, Y.; Wren, A.W. Copper-containing glass polyalkenoate cements based on SiO 2-ZnO-CaO-SrO-P 2 O 5 glasses: Glass characterization, physical and antibacterial properties. *J. Mater. Sci.* **2017**, *52*, 8886–8903. [CrossRef]
26. Niccolai, A.; Caputo, D.; Chieco, L.; Grimaccia, F.; Mussetta, M. Machine Learning-Based Detection Technique for NDT in Industrial Manufacturing. *Mathematics* **2021**, *9*, 1251. [CrossRef]
27. Versaci, M.; Angiulli, G.; Di Barba, P.; Morabito, F.C. Joint use of eddy current imaging and fuzzy similarities to assess the integrity of steel plates. *Open Phys.* **2020**, *18*, 230–240. [CrossRef]
28. Burrascano, P.; Ciuffetti, M. Early Detection of Defects through the Identification of Distortion Characteristics in Ultrasonic Responses. *Mathematics* **2021**, *9*, 850. [CrossRef]
29. Chon, S.S.; Piraino, L.; Mokhtari, S.; Krull, E.A.; Coughlan, A.; Gong, Y.; Wren, A.W. Synthesis, characterization and solubility analysis of amorphous SiO2-CaO-Na2O-P2O5 scaffolds for hard tissue repair. *J. Non-Cryst. Solids* **2018**, *490*, 1–12. [CrossRef]
30. Faba, A.; Antonio, S.Q. An Overview of Non-Destructive Testing of Goss Texture in Grain-Oriented Magnetic Steels. *Mathematics* **2021**, *9*, 1539. [CrossRef]
31. Mokhtari, S.; Krull, E.A.; Sanders, L.M.; Coughlan, A.; Mellott, N.P.; Gong, Y.; Wren, A.W. Investigating the effect of germanium on the structure of SiO2-ZnO-CaO-SrO-P2O5 glasses and the subsequent influence on glass polyalkenoate cement formation, solubility and bioactivity. *Mater. Sci. Eng. C* **2019**, *103*, 109843. [CrossRef]
32. Khounani, Z.; Hosseinzadeh-Bandbafha, H.; Nazemi, F.; Shaeifi, M.; Karimi, K.; Tabatabaei, M.; Aghbashlo, M.; Lam, S.S. Exergy analysis of a whole-crop safflower biorefinery: A step towards reducing agricultural wastes in a sustainable manner. *J. Environ. Manag.* **2021**, *279*, 111822. [CrossRef]
33. Roshani, G.; Nazemi, E.; Roshani, M. Usage of two transmitted detectors with optimized orientation in order to three phase flow me-tering. *Measurement* **2017**, *100*, 122–130. [CrossRef]
34. Hosseinzadeh-Bandbafha, H.; Nazemi, F.; Khounani, Z.; Ghanavati, H.; Shafiei, M.; Karimi, K.; Lam, S.S.; Aghbashlo, M.; Tabatabaei, M. Safflower-based biorefinery producing a broad spectrum of biofuels and biochemicals: A life cycle assessment perspective. *Sci. Total. Environ.* **2021**, *802*, 149842. [CrossRef]
35. Roshani, G.; Nazemi, E.; Roshani, M. Intelligent recognition of gas-oil-water three-phase flow regime and determination of volume fraction using radial basis function. *Flow Meas. Instrum.* **2017**, *54*, 39–45. [CrossRef]
36. Samimi, A. Risk Management in Oil and Gas Refineries. *Prog. Chem. Biochem. Res.* **2020**, *3*, 140–146. [CrossRef]
37. Nazemi, F.; Karimi, K.; Denayer, J.F.; Shafiei, M. Techno-economic aspects of different process approaches based on brown macroalgae feedstock: A step toward commercialization of seaweed-based biorefineries. *Algal. Res.* **2021**, *58*, 102366. [CrossRef]
38. Roshani, S.; Roshani, S. Design of a high efficiency class-F power amplifier with large signal and small signal measurements. *Measurement* **2020**, *149*, 106991. [CrossRef]
39. Pourbemany, J.; Mirjalily, G.; Abouei, J.; Raouf, A.H.F. Load Balanced Ad-Hoc On-Demand Routing Basedon Weighted Mean Queue Length Metric. In Proceedings of the Electrical Engineering (ICEE), Iranian Conference on IEEE, Mashhad, Iran, 8–10 May 2018; pp. 470–475. [CrossRef]
40. Pirasteh, A.; Roshani, S.; Roshani, S. A modified class-F power amplifier with miniaturized harmonic control circuit. *AEU Int. J. Electron. Commun.* **2018**, *97*, 202–209. [CrossRef]
41. Jamshidi, M.B.; Roshani, S.; Talla, J.; Roshani, S.; Peroutka, Z. Size reduction and performance improvement of a microstrip Wilkinson power divider using a hybrid design technique. *Sci. Rep.* **2021**, *11*, 1–15. [CrossRef] [PubMed]
42. Jamshidi, M.B.; Siahkamari, H.; Roshani, S.; Roshani, S. A compact Gysel power divider design using U-shaped and T-shaped reso-nators with harmonics suppression. *Electromagnetics* **2019**, *39*, 491–504. [CrossRef]
43. Roshani, S.; Roshani, S.; Zarinitabar, A. A modified Wilkinson power divider with ultra harmonic suppression using open stubs and lowpass filters. *Analog. Integr. Circuits Signal Process.* **2019**, *98*, 395–399. [CrossRef]
44. Roshani, S.; Roshani, S. Design of a very compact and sharp bandpass diplexer with bended lines for GSM and LTE applications. *AEU Int. J. Electron. Commun.* **2019**, *99*, 354–360. [CrossRef]
45. Roshani, S.; Roshani, S. A compact coupler design using meandered line compact microstrip resonant cell (MLCMRC) and bended lines. *Wireless Networks* **2021**, *27*, 677–684. [CrossRef]
46. Pirasteh, A.; Roshani, S.; Roshani, S. Compact microstrip lowpass filter with ultrasharp response using a square-loaded modified T-shaped resonator. *Turk. J. Electr. Eng. Comput. Sci.* **2018**, *26*, 1736–1746. [CrossRef]
47. Mokhtari, S.; Wren, A.W. Investigating the effect of copper addition on SiO2-ZnO-CaO-SrO-P2O5 glass polyalkenoate cements: Physical, mechanical and biological behavior. *Biomed. Glasses* **2019**, *5*, 13–33. [CrossRef]

48. Shekouhi, N.; Dick, D.; Baechle, M.W.; Kaeley, D.K.; Goel, V.K.; Serhan, H.; Rawlinson, J.; Shaw, D. Clinically relevant finite element technique based protocol to evaluate growing rods for early onset scoliosis correction. *JOR Spine* **2020**, *3*, 1119. [CrossRef]
49. Kumar, V.; Kumar, A. Self-reliance in advanced diagnostic imaging for accessible, affordable, and quality health care in India. *J. Nat. Sci. Biol. Med.* **2021**, *12*, 129. [CrossRef]
50. Sowndarya, K.; Joseph, J.A.; Shenoy, A.; Hegde, A. Evaluation of triglyceride/high-density lipoprotein ratio as a surrogate marker for insulin resistance in healthy young males. *J. Nat. Sci. Biol. Med.* **2021**, *12*, 213. [CrossRef]
51. Khayatnezhad, M.; Nasehi, F. Industrial pesticides and a methods assessment for the reduction of associated risks: A Review. *Adv. Life Sci.* **2021**, *8*, 202–210.
52. Sengodan, V.C.; Appusamy, N. Comparative anthropometry analysis of the digital X-rays of the right and left hip joints in an Indian population. *J. Nat. Sci. Biol. Med.* **2020**, *11*, 3. [CrossRef]
53. Ashrafi, R.; Azarbayjani, M.; Cox, R.; Futrell, B.; Glass, J.; Zarrabi, A.; Amirazar, A. Assessing the Performance of UFAD System in an Office Building Located in Various Climate Zones. In Proceedings of the Symposium on Simulation for Architecture and Urban Design, Atlanta, Georgia, 7–9 April 2019.
54. Moradi, M.J.; Hariri-Ardebili, M.A. Developing a Library of Shear Walls Database and the Neural Network Based Predictive Meta Model. *Appl. Sci.* **2019**, *9*, 2562. [CrossRef]
55. Nazemi, B.; Rafiean, M. Forecasting house prices in Iran using GMDH. *Int. J. Hous. Mark. Anal.* **2021**, *14*, 555–568. [CrossRef]
56. Moradi, M.J.; Roshani, M.M.; Shabani, A.; Kioumarsi, M. Prediction of the Load-Bearing Behavior of SPSW with Rectangular Opening by RBF Network. *Appl. Sci.* **2020**, *10*, 1185. [CrossRef]
57. David, O.O.; Grobler, W. Age Progression, Social Interventions and Food Insecurity In South Africa: Logistic Regression Analysis. *Int. J. Soc. Sci. Humanit. Stud.* **2020**, *12*, 289–305.
58. Igbokwe-Ibeto, C.J. Analysing the interface between bureaucracy, interest groups, and public policymaking for good governance in africa. *Int. J. Bus. Manag. Stud.* **2020**, *12*, 2.
59. Adewumi, S.A. Challenges and Prospects of Rural Entrepreneurship: A Discourse Analysis Of Selected Local Government Areas Of Osun State. *IJBS* **2020**, *12*, 544–560.
60. Danielle, N.E.L.; Masilela, L. Open Governance for Improved Service Delivery Innovation In South Africa. *Int. J. eBusiness eGovernment Stud.* **2020**, *12*, 33–47.
61. Dubois, O.; Silvius, G. The Relation Between Sustainable Project Management and Project Success. *Relation* **2020**, *9*, 218–238. [CrossRef]
62. Mao, C.C.; Ma, Z.X. The analysis of the regional economic growth and the regional financial industry development difference in china based on the theil index. *Int. J. Econ. Financ. Stud.* **2021**, *13*, 128–154.
63. Hartani, N.H.; Haron, N.; Tajuddin, N.I.I. The impact of strategic alignment on the sustainable com-petitive advantages: Mediating role of it implementation success and it managerial resource. *Int. J. eBusiness eGovernment Stud.* **2021**, *2021 13*, 78–96.
64. Jassim, T.L. The Influence of Oil Prices, Licensing and Production on the Economic Development: An Empirical Investigation of Iraq Economy. *J. Agrobiotechnology Manag. Econ.* **2021**, *23*, 1–11.
65. Hassan, A.S.; Meyer, D.F. Analysis of The Non-Linear Effect of Petrol Price Changes on Inflation in South Africa. *Int. J. Soc. Sci. Humanit. Stud.* **2020**, *12*, 34–49.
66. Rerksuppaphol, L.; Rerksuppaphol, S. Comparison of equations for the calculation of low-density lipoprotein cholesterol in thai population. *J. Nat. Sci. Biol. Med.* **2021**, *12*, 224. [CrossRef]
67. Dunga, H.M. An empirical analysis on determinants of food security among female-headed households in South Africa. *International J. Soc. Sci. Humanit. Stud.* **2020**, *12*, 66–81.
68. Talha, M.; Sohail, M.; Tariq, R.; Ahmad, M.T. Impact of Oil Prices, Energy Consumption and Economic Growth on the Inflation Rate in Malaysia. *Cuad. Econ.* **2021**, *44*, 26–32.
69. Karami, A.; Roshani, G.H.; Nazemi, E.; Roshani, S. Enhancing the performance of a dual-energy gamma ray based three-phase flow meter with the help of grey wolf optimization algorithm. *Flow Meas. Instrum.* **2018**, *64*, 164–172. [CrossRef]
70. Moosaie, A.; Shekouhi, N.; Nouri, N.M.; Manhart, M. An algebraic closure model for the DNS of turbulent drag reduction by Brownian microfiber additives in a channel flow. *J. Non-Newtonian Fluid Mech.* **2015**, *226*, 60–66. [CrossRef]
71. Roshani, G.; Nazemi, E. Intelligent densitometry of petroleum products in stratified regime of two phase flows using gamma ray and neural network. *Flow Meas. Instrum.* **2017**, *58*, 6–11. [CrossRef]
72. Mosorov, V.; Rybak, G.; Sankowski, D. Plug Regime Flow Velocity Measurement Problem Based on Correlability Notion and Twin Plane Electrical Capacitance Tomography: Use Case. *Sensors* **2021**, *21*, 2189. [CrossRef] [PubMed]
73. Roshani, G.H.; Roshani, S.; Nazemi, E.; Roshani, S. Online measuring density of oil products in annular regime of gas-liquid two phase flows. *Measurement* **2018**, *129*, 296–301. [CrossRef]
74. Roshani, G.; Hanus, R.; Khazaei, A.; Zych, M.; Nazemi, E.; Mosorov, V. Density and velocity determination for single-phase flow based on radiotracer technique and neural networks. *Flow Meas. Instrum.* **2018**, *61*, 9–14. [CrossRef]
75. Taylan, O.; Sattari, M.A.; Elhachfi Essoussi, I.; Nazemi, E. Frequency Domain Feature Extraction Investigation to Increase the Accuracy of an Intelligent Nondestructive System for Volume Fraction and Regime Determination of Gas-Water-Oil Three-Phase Flows. *Mathematics* **2021**, *9*, 2091. [CrossRef]
76. Roshani, G.H.; Nazemi, E.; Feghhi, S.A.H. Investigation of using 60 Co source and one detector for determining the flow regime and void fraction in gas–liquid two-phase flows. *Flow Meas. Instrum.* **2016**, *50*, 73–79. [CrossRef]

77. Pourbemany, J.; Zhu, Y.; Bettati, R. Breath to Pair (B2P): Respiration-Based Pairing Protocol for Wearable Devices. *arXiv preprint* **2021**, arXiv:2107.11677.
78. Roshani, S.; Roshani, S. Two-Section Impedance Transformer Design and Modeling for Power Amplifier Applications. *Appl. Comput. Electromagn. Soc. J.* **2017**, *32*, 1042–1047.
79. Pourbemany, J.; Zhu, Y.; Bettati, R. A Survey of Wearable Devices Pairing Based on Biometric Signals. *arXiv preprint* **2021**, arXiv:2107.11685.
80. Rezaei, T.; Aslmarand, S.M.; Snyder, R.; Khajavi, B.; Alsing, P.M.; Fanto, M.; Miller, W.A. Experimentalrealization of Schumacher's information geometric Bell inequality. *Phys. Lett. A* **2021**, *405*, 127–444. [CrossRef]
81. Roshani, G.; Nazemi, E.; Roshani, M. Identification of flow regime and estimation of volume fraction independent of liquid phase density in gas-liquid two-phase flow. *Prog. Nucl. Energy* **2017**, *98*, 29–37. [CrossRef]
82. Karami, A.; Roshani, G.H.; Khazaei, A.; Nazemi, E.; Fallahi, M. Investigation of different sources in order to optimize the nuclear metering system of gas–oil–water annular flows. *Neural Comput. Appl.* **2018**, *32*, 3619–3631. [CrossRef]
83. Hanus, R.; Zych, M.; Mosorov, V.; Golijanek, J.; Jedrzejczyk, A.; Jaszczur, M.; Andruszkiewicz, A. Evaluation of liquid-gas flow in pipeline using gamma-ray absorption technique and advanced signal processing. *Metrol. Meas. Syst.* **2021**, *28*, 145–159.
84. Roshani, G.H.; Nazemi, E.; Roshani, M.M. Flow regime independent volume fraction estimation in three-phase flows using dual-energy broad beam technique and artificial neural network. *Neural Comput. Appl.* **2016**, *28*, 1265–1274. [CrossRef]
85. Hanus, R.; Zych, M.; Kusy, M.; Jaszczur, M.; Petryka, L. Identification of liquid-gas flow regime in a pipeline using gamma-ray ab-sorption technique and computational intelligence methods. *Flow Meas. Instrum.* **2018**, *60*, 17–23. [CrossRef]
86. Roshani, G.H.; Nazemi, E.; Feghhi, S.A.; Setayeshi, S. Flow regime identification and void fraction prediction in two-phase flows based on gamma ray attenuation. *Measurement* **2015**, *62*, 25–32. [CrossRef]
87. Alkabaa, A.S.; Nazemi, E.; Taylan, O.; Kalmoun, E.M. Application of Artificial Intelligence and Gamma Attenuation Techniques for Predicting Gas–Oil–Water Volume Fraction in Annular Regime of Three-Phase Flow Independent of Oil Pipeline's Scale Layer. *Mathematics* **2021**, *9*, 1460. [CrossRef]
88. Sattari, M.A.; Roshani, G.H.; Hanus, R.; Nazemi, E. Applicability of time-domain feature extraction methods and artificial intelligence in two-phase flow meters based on gamma-ray absorption technique. *Measurement* **2021**, *168*, 108474. [CrossRef]
89. Basahel, A.; Sattari, M.; Taylan, O.; Nazemi, E. Application of Feature Extraction and Artificial Intelligence Techniques for Increasing the Accuracy of X-ray Radiation Based Two Phase Flow Meter. *Mathematics* **2021**, *9*, 1227. [CrossRef]
90. Roshani, G.H.; Feghhi, S.A.H.; Mahmoudi-Aznaveh, A.; Nazemi, E.; Adineh-Vand, A. Precise volume fraction prediction in oil–water–gas multiphase flows by means of gamma-ray attenuation and artificial neural networks using one detector. *Measurement* **2014**, *51*, 34–41. [CrossRef]
91. He, Y.; Tsang, K.F.; Kong, R.Y.-C.; Chow, Y.-T. Indication of Electromagnetic Field Exposure via RBF-SVM Using Time-Series Features of Zebrafish Locomotion. *Sensors* **2020**, *20*, 4818. [CrossRef] [PubMed]
92. Juliani, C.; Ellefmo, S.L. Prospectivity Mapping of Mineral Deposits in Northern Norway Using Radial Basis Function Neural Networks. *Minerals* **2019**, *9*, 131. [CrossRef]
93. Broomhead, D.S.; Lowe, D. Multivariable functional interpolation and adaptive networks. *Complex Syst.* **1988**, *2*, 321–355.
94. Moody, J.E.; Darken, C.J. Fast Learning in Networks of Locally-Tuned Processing Units. *Neural Comput.* **1989**, *1*, 281–294. [CrossRef]